

Enhancing Visual Conditioning via Track-Following Preference Optimization in Vision-Language-Action Models

Yiye Chen^{1†} Yanan Jian^{2‡} Xiaoyi Dong³ Shuxin Cao¹ Jing Wu^{4†} Patricio Vela¹ Benjamin E. Lundell^{5‡}
Dongdong Chen³

Abstract

Vision-Language-Action (VLA) models have demonstrated strong performance across a wide range of robotic manipulation tasks. Despite the success, extending large pretrained Vision-Language Models (VLMs) to the action space can induce vision-action misalignment, where action predictions exhibit weak dependence on the current visual state, leading to unreliable action outputs. In this work, we study VLA models through the lens of visual conditioning and empirically show that successful rollouts consistently exhibit stronger visual dependence than failed ones. Motivated by this observation, we propose a training framework that explicitly strengthens visual conditioning in VLA models. Our approach first aligns action prediction with visual input via preference optimization on a track-following surrogate task, and then transfers the enhanced alignment to instruction-following task through latent-space distillation during supervised finetuning. Without introducing architectural modifications or additional data collection, our method improves both visual conditioning and task performance for discrete OpenVLA, and further yields consistent gains when extended to the continuous OpenVLA-OFT setting. Project website: <https://vista-vla.github.io/>.

1. Introduction

Recent research has shown increasing interest in the important challenge of developing instruction-following robots capable of completing manipulation tasks conditioned on natural language commands (Chen et al., 2021; Huang et al., 2022; Shridhar et al., 2022; 2023). Vision-Language-Action

[†]Work done during an internship at Microsoft. [‡]Work done while working at Microsoft. ¹Georgia Tech ²Nvidia ³Microsoft ⁴University of Oxford ⁵ARM. Correspondence to: Yiye Chen <yychen2019@gatech.edu>.

Preprint. February 6, 2026.

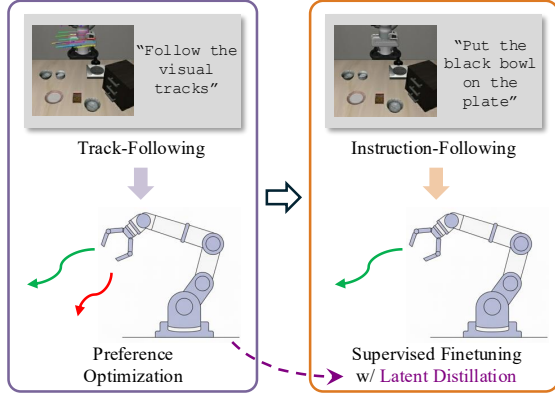


Figure 1. VISTA Overview. We align VLA action outputs to visual tracks via preference optimization, followed by supervised finetuning with latent distillation. Our experiments show that VISTA enhances visual conditioning and improves performance.

(VLA) models seek to address this challenge by extending large Vision-Language Models (VLMs) with action prediction modules. This paradigm seeks to transfer the rich perceptual and reasoning capabilities learned during VLM pretraining to embodied action prediction.

Despite the current success, it remains unclear to what extent the world knowledge and visual understanding encoded in VLMs effectively propagates to the VLA. Recent studies (Zhang et al., 2025; Yuan et al., 2025) suggest that information extracted from VLMs may be insufficient for embodied decision-making, due to the discrepancy of the feature granularity required by the vision-language reasoning and visuomotor control. Other work (Kachaev et al., 2025; Driess et al., 2025) further shows the degradation in the visual representation due to finetuning on the extended action output domain. These findings point to the potential *misalignment* between perceptual understanding and action generation, wherein policies underutilize visual evidence and instead rely on spurious priors, resulting in unreliable action outputs. To mitigate this issue, existing approaches introduce auxiliary tasks, such as video prediction (Wu et al., 2024; Hu et al., 2025), dynamics understanding (Bu et al., 2025; Ye et al., 2024; Chen et al., 2025a), spatial question answering (Black et al., 2025; Zhou et al., 2025), and distil-

lation from external experts (Dong et al., 2025), to enhance fine-grained visual understanding. However, despite the incurred substantial training cost, it remains unclear how those external knowledge translates to better action prediction, as their impact on the policy decision is hard to characterize.

In this paper, we study the problem through the novel lens of *visual conditioning*, which explicitly measures the extent of the impact of visual clue on the action prediction. Intuitively, stronger visual conditioning is desirable for VLA models, as weak conditioning might indicate insufficient consideration of the current state and poor utilization of the VLM knowledge, leading to brittle action outputs. To consolidate this notion, we quantify visual conditioning by measuring the shift in the predicted action distribution under the distortion of the visual input. Under this formulation, we empirically demonstrate on the state-of-the-art VLA that successful rollouts exhibit stronger visual conditioning than failure ones, which validates the significance of visual conditioning for robust action generation.

Based on this observation, we aim to improve VLA performance by explicitly strengthening visual conditioning during action prediction. Our approach is motivated by the success of *preference optimization* in mitigating VLMs hallucinations, where training on pairs of preferred and dispreferred responses encourages stronger reliance on visual evidence (Peng et al., 2025; Zhou et al., 2024a; Ouali et al., 2024). However, extending preference optimization to instruction-following VLA policies is non-trivial, as constructing meaningful preference pairs requires dispreferred action chunks that are both in-distribution and less likely to accomplish the task. This necessitates costly on-policy rollouts and expert-defined trajectory ranking (Zhang et al., 2024), which limits scalability and flexibility.

To address this challenge, we propose **VISTA**: *Improving Visuomotor Coordination by Aligning Visual Tracks and Actions in VLA*. The core idea of VISTA is to leverage visual tracks to make vision–action correspondence explicit, thereby enabling principled construction of preference pairs without model rollouts. As illustrated in Figure 1, VISTA augments standard supervised fine-tuning (SFT) with two additional training stages. In the first stage, we apply Direct Preference Optimization (Rafailov et al., 2023) to the *track-following* task, where the VLA model predicts actions based on track-annotated images. The track-following data are readily constructed from the instruction-following dataset by annotating the image with pixel tracks and applying minimal prompt modifications. Preference pairs are then constructed entirely offline via in-batch pairing, which treats action chunks from other samples within the same batch as dispreferred responses. We show that the track-following DPO implicitly optimizes inverse dynamics understanding in the VLA policy and greatly improves visual conditioning

during action prediction. In the second stage, VISTA performs instruction-following SFT with feature-space distillation from the frozen track-following model, which leverages the correspondence between the two tasks to transfer the enhanced visual grounding to the target task.

Without introducing architectural changes, auxiliary datasets, or on-policy rollouts, VISTA consistently improves visual conditioning and performance in the vanilla discrete autoregressive VLA model. In particular, it improves OpenVLA (Kim et al., 2024) by 3.15% in average success rate on the LIBERO benchmark, demonstrating the benefit of strengthening visual conditioning through training. Moreover, we also show that our method naturally extends to continuous parallel-decoding architectures by modifying only the final training stage. This simple extension improves OpenVLA-OFT (Kim et al., 2025) on Calvin ABC→D from 3.87 to 4.02 in average task completion count, corresponding to a 4% relative improvement.

In summary, our contributions are:

- We study Vision-Language-Action (VLA) models through the novel lens of *visual conditioning* and demonstrate its importance for VLA performance.
- We introduce VISTA, a new training framework that improves visual conditioning in VLA policies by aligning action predictions to visual tracks.
- We show that VISTA enhances visual conditioning and consistently improves the performance of both discrete OpenVLA and continuous OpenVLA-OFT on standard benchmarks.

2. Related Works

Vision-Language-Action Models Early work in robot learning leverages vision and language foundation models as modular components within larger systems (Yang et al., 2023; Rana et al., 2023; Chen et al., 2025b; Huang et al., 2023). More recent efforts instead focus on endowing large pretrained Vision–Language Models (VLMs) with end-to-end action prediction capabilities. By tokenizing actions through discretization (Brohan et al., 2022; Kim et al., 2024) or frequency decomposition (Pertsch et al., 2025), the vanilla discrete autoregressive VLA models achieve strong performance powered by large-scale action-labeled datasets (Wang et al., 2024; Black et al., 2025). Moderate architectural extensions, such as continuous-action experts (Kim et al., 2025; Wang et al., 2025a; Li et al., 2024) and parallel-decoding schemes (Kim et al., 2025; Zhao et al., 2025), have further improved the model expressivity and performance.

Despite the progress, recent studies report lack of fine-grained visual feature in VLM for embodied tasks (Zhang

et al., 2025; Hancock et al., 2025; Yuan et al., 2025; Chen et al., 2024) or degraded multimodal representation during VLA finetuning (Kachaev et al., 2025; Dong et al., 2025; Driess et al., 2025). A broad line of work seeks to address the issue by injecting world knowledge into VLAs, through the task of latent action modeling (Chen et al., 2025a; Ye et al., 2024; Bu et al., 2025), embodied vision-language reasoning (Zhou et al., 2025; Zawalski et al., 2024), dynamic modeling (Wang et al., 2025b; Li et al., 2025; Bi et al., 2025), or video prediction (Zhao et al., 2025; Bu et al., 2024b; Black et al., 2024; Wu et al., 2024). However, these approaches rely on auxiliary objectives whose impact on instruction-following action prediction is indirect and difficult to quantify, especially given separate training stages or distinct internal computation paths. In contrast, we explicitly quantifies visual clue utilization in action generation, and propose a training method to enhance visual grounding.

Visual Track Guidance in Robot Learning Visual tracks, which depict pixel-level trajectories, have been widely used as a general representation of scene dynamics across diverse applications (Zholus et al., 2025; Geng et al., 2025). In robotics, visual track has facilitated policy training by serving as intermediate motion representations (Wen et al., 2023; Bharadhwaj et al., 2024) and enabling the extraction of dynamic knowledge from generic video data (Ren et al., 2025). In the context of VLA models, LLARVA (Niu et al., 2024) employs future track prediction as an auxiliary objective, while TraceVLA (Zheng et al., 2024) uses visual tracks to represent historical action context. In contrast, we leverage visual tracks to formulate a preference optimization objective to align action prediction with visual input.

Multimodal Alignment and Preference Optimization Multimodal misalignment is a central challenge for large multimodal models. In Vision Language Models (VLMs), such misalignment often manifests as underutilization of visual input, leading to hallucinated output (Shu et al., 2025; Liu et al., 2023b). Preference optimization has emerged as an effective strategy to address the issue, in which the models are trained on paired preferred and dispreferred responses for stronger visual grounding (Zhou et al., 2024a; Zhao et al., 2023; Ouali et al., 2024; Zhou et al., 2024b). In this paper, we study VLAs through the same lens, by showing the connection between visual conditioning and action prediction performance. Building on this insight, we introduce a preference optimization framework that aligns action prediction with visual input, strengthening visual grounding and improving downstream performance.

3. Visual Conditioning in VLA Models

3.1. VLA Preliminaries

Problem Formulation We consider the problem of building a VLA model π_θ , parameterized by θ , which processes a language instruction g and a third-person RGB observation o_t at time step t , and outputs a chunk of H actions $a_{t:t+H}$:

$$a_{t:t+H} = \pi_\theta(o_t, g) \quad (1)$$

Although some work incorporates additional inputs such as robot proprioception and wrist-camera images, we exclude those modalities in all experiments for fair comparison.

Standard VLA Structures The VLA model π consists of a multimodal backbone f that encodes inputs into a set of M latents, followed by an action expert ϕ that maps these latents to the actions. Two main categories of ϕ involve: Existing VLA approaches broadly fall into two representative categories based on the design of attention in f and architecture of ϕ : (1) Vainlla *autoregressive discrete* formulation, which inherits the autoregressive backbone and token classification head from VLMs and outputs a distribution over a set of discrete action tokens: $a_{t:t+H} \sim \pi(\cdot|o_t, g)$; (2) Extended *parallel-decoding continuous* formulation, which adopts parallel-decoding attention and replaces the token head with a regression expert from the scratch that directly outputs the actions: $a_{t:t+H} = \pi(o_t, g)$.

In this work, we study training method under both formulations through OpenVLA (Kim et al., 2024) and OpenVLA-OFT (Kim et al., 2025) architectures. In both cases, f is finetuned from Prismatic VLM (Karamcheti et al., 2024), and each output latent corresponds to one action dimension, leading to $M = 7H$ for a standard 7-DoF action space (translation, rotation, gripper). OpenVLA instantiates the autoregressive discrete formulation, whereas OpenVLA-OFT realizes the parallel-decoding continuous scheme, where ϕ is implemented as a 4-layer MLP network.

Instruction-following Dataset Training of a VLA requires an instruction-following dataset $\mathcal{D} = \{(\zeta, g)\}$, where the trajectory ζ records a sequence of actions and observations to accomplish the task g given initial observation o_1 : $\zeta = \{(o_t, a_t)\}_{t=1}^T$. The trajectories are further segmented into action chunks of fixed length H via sliding window, which supervises the outputs of VLA formulated in Eq. 1.

3.2. Quantifying Visual Conditioning

Inspired by Visual Contrastive Decoding (VCD) (Leng et al., 2024), we probe visual conditioning in the autoregressive discrete VLA by measuring the sensitivity of action predictions to visual input. Formally, we define the visual conditioning at token position τ as the KL-divergence between the predicted action token distributions conditioned

on the original and perturbed observations, respectively:

$$D_{\text{KL}}(\pi(\cdot|o_t, g, a_t^{<\tau})||\pi(\cdot|o'_t, g, a_t^{<\tau}))$$

$$a_t^{<\tau} \sim \pi(\cdot|o_t, g), \quad \tau = 1, \dots, M \quad (2)$$

where $a_t^{<\tau}$ are predicted tokens prior to position τ . o'_t is the distorted image based on o_t . We follow VCD to implement the distortion as the forward diffusion process (Ho et al., 2020), by repetitively shrinking the original image and adding Gaussian noise for K step. Equivalently, o'_t is sampled from the following distribution:

$$q(o_t^k|o_t^{k-1}) = \mathcal{N}(o_t^k; \sqrt{1 - \beta_k} o_t^{k-1}, \beta_k \mathbf{I}),$$

$$q(o'_t|o_t) = \prod_{k=1}^K q(o_t^k|o_t^{k-1}), \quad o_t^0 = o_t \quad (3)$$

where \mathbf{I} refers to an identity matrix. We follow VCD to set $K = 999$ and schedule the variance linearly from $\beta_1 = 10^{-5}$ to $\beta_K = 0.005$.

3.3. Visual Conditioning and VLA Performance

We begin by probing visual conditioning in OpenVLA fine-tuned on LIBERO-Spatial benchmark (Sec. 5.1.1) with chunk size $H = 8$ (i.e. $M = 56$). Using the definition in Eq. (2), we measure visual conditioning across all output tokens over 100 rollouts (10 tasks with 10 rollouts per task). Rollouts are categorized into successful and failed groups based on simulation outcomes, and we report the mean and standard deviation aggregated over time steps and rollouts.

As shown in Figure 2, successful rollouts consistently exhibit stronger visual conditioning than failed ones. This gap is most pronounced for early action tokens, which depend more heavily on visual input due to limited preceding token predictions. These results establish a clear correlation between visual conditioning and VLA performance, which supports our notion that effective VLA policy requires strong visual grounding. Motivated by the observation, we design a training approach to explicitly enhance vision-action alignment in Sec. 4. As previewed in Figure 2, our method increases visual conditioning in OpenVLA, and leads to consistent performance improvement across multiple benchmarks as discussed in Sec. 5.

4. Methodology

As illustrated in Figure 3, VISTA involves 3 training stages. In Stage 0, we begin with standard instruction-following supervised fine-tuning (SFT) on a discrete autoregressive VLA, which provides a base model for the subsequent stages. In Stage 1 (Sec. 4.1), we produce track-following data from the instruction-following dataset \mathcal{D} and apply Direct Preference Optimization (DPO) to enhance vision-action alignment. In Stage 2 (Sec. 4.2), we propagate the enhanced

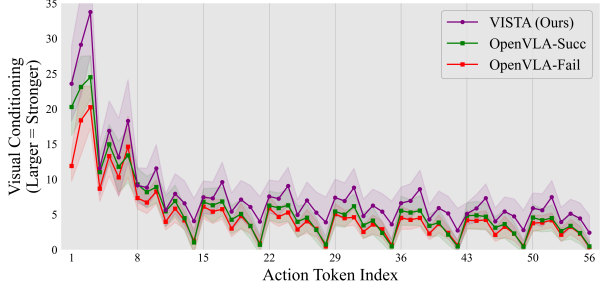


Figure 2. **Visual Conditioning of the 8-step OpenVLA and VISTA (Ours) in LIBERO-Spatial.** The periodic vertical grids indicate that each block of seven tokens decodes to a single action, leading to 56 output tokens for 8 actions.

alignment to the instruction-following task of interest by additional SFT with latent distillation from the frozen copy of track-aligned VLA.

4.1. Track-Follow Preference Optimization

4.1.1. TRACK-FOLLOWING DPO DESIGN

Track-following Preference Dataset Construction. This stage starts from a base instruction-following VLA model to improve its visual conditioning via preference optimization. To avoid the need for costly on-policy rollouts and expert-defined rewards when defining preference pairs for instruction-following tasks (Zhang et al., 2024), we instead formulate preference optimization for the *track-following* task, where the action prediction is guided by the annotated tracks on the image. These tracks establish deterministic correspondence between visual input and action chunks output, enabling principled preference construction directly from the offline instruction-following dataset \mathcal{D} .

We first construct a track-following dataset $\tilde{\mathcal{D}}$ by annotating \mathcal{D} . Specifically, for each time step t within trajectory ζ , we employ an off-the-shelf point tracking model to track N points over the next H frames $(o_t, o_{t+1}, \dots, o_{t+\min(t+H-1, T)})$. Following TraceVLA (Zheng et al., 2024) we retain only the active points by filtering based on L1 moving distances, and then randomly sample n active tracks. These tracks are overlaid on the initial frame o_t to produce a track-annotated image \tilde{o}_t , which depicts both the current state and the future dynamics given the labeled actions. By repeating the process for all frames in \mathcal{D} , we obtain the track-following dataset $\tilde{\mathcal{D}} = \{(\tilde{\zeta}, \tilde{g})\}$, where the track-annotated trajectory $\tilde{\zeta} = \{(\tilde{o}_t, a_t)\}_{t=1}^T$, and \tilde{g} is the updated prompt as shown in Figure 3.

We then construct track-following preference pairs on $\tilde{\mathcal{D}}$ via *in-batch preference pairing*. Since visual tracks deterministically specify the preferred actions, action chunks drawn from other batch samples can naturally serve as in-distribution yet visually misaligned responses. Concretely, given a randomly shuffled track-following batch

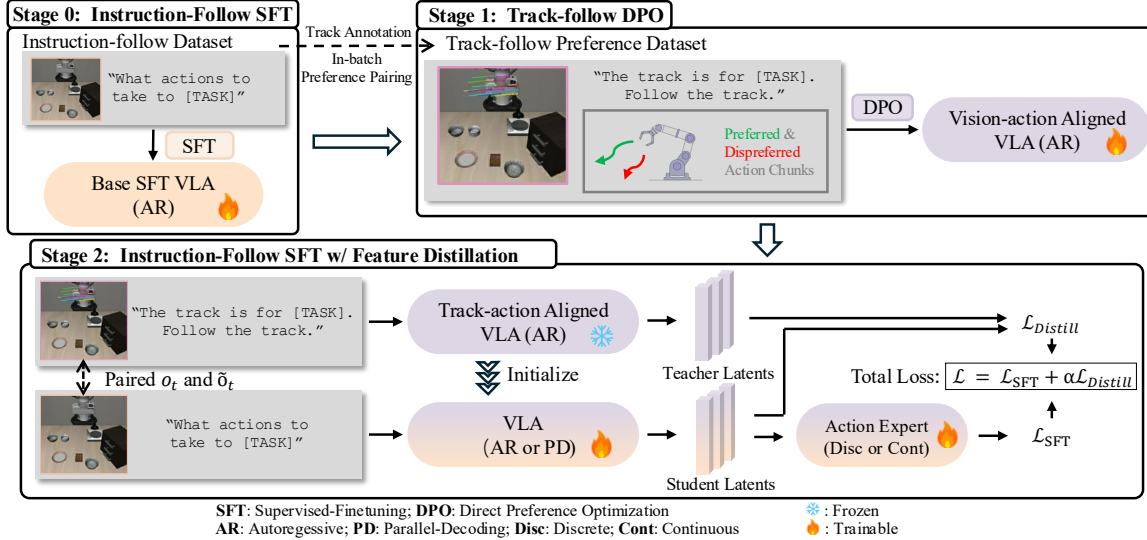


Figure 3. VISTA Methodology. Starting from a vanilla instruction-following SFT model, we apply DPO on track-following preference samples constructed from the instruction-following dataset to align action prediction with visual input. We then transfer the alignment to the instruction-following policy via latent distillation, resulting in enhanced visual conditioning and VLA performance.

$\{(\tilde{o}_t^b, \tilde{g}^b, a_{t:t+H}^b)\}_{b=1}^B$, where B is set as even, we create the preference batch $\{(\tilde{o}_t^b, \tilde{g}^b, a_w^b, a_l^b)\}_{b=1}^B$, where the preferred a_w^b and dispreferred a_l^b are set as:

$$a_w^b = a_{t:t+H}^b, \quad a_l^b = \begin{cases} a_{t:t+H}^{b+1}, & \text{if } b \text{ is odd} \\ a_{t:t+H}^{b-1}, & \text{if } b \text{ is even} \end{cases} \quad (4)$$

Track-following DPO Formulation With the track-following preference data, we align action predictions to visual tracks via Direct Preference Optimization (DPO) (Rafailov et al., 2023). We optimize the objective:

$$\mathcal{L}_{trackDPO}(\pi_\theta) = -\mathbb{E}_{(\tilde{o}, \tilde{g}, a_w, a_l) \sim \tilde{\mathcal{D}}} \left[\log \sigma \left(\alpha \left(\log \frac{\pi_\theta(a_w; \tilde{o}, \tilde{g})}{\pi_{ref}(a_w; \tilde{o}, \tilde{g})} - \log \frac{\pi_\theta(a_l; \tilde{o}, \tilde{g})}{\pi_{ref}(a_l; \tilde{o}, \tilde{g})} \right) \right) \right] \quad (5)$$

where σ denotes the logistic function and α controls the deviation from the reference policy π_{ref} , which is fixed as the frozen Stage 0 SFT model. Here, $\pi(a; \tilde{o}, \tilde{g})$ is the conditional likelihood of an action chunk estimated by the autoregressive VLA model, which is calculated as the sequential product of the token-level probabilities from the model outputs. By contrasting against preferred and dispreferred action chunks based on the visual track guidance, DPO encourages the policy to align predictions with visual evidence, thereby strengthening the visual conditioning.

4.1.2. TRACK-FOLLOWING DPO IMPLICITLY TRAINS INVERSE DYNAMICS UNDERSTANDING

Unlike prior approaches that explicitly learn inverse dynamics that recover actions based on the current and future states

(Du et al., 2023; Tian et al., 2024), we show that our designed DPO program implicitly achieves this. As derived in Rafailov et al. (2023), the DPO program in Eq. 5 implicitly optimizes the following RL objective:

$$\mathcal{L}(\pi_\theta) = -\mathbb{E}_{(a, \tilde{o}, \tilde{g}) \sim \tilde{\mathcal{D}}} \left[r(a, \tilde{o}, \tilde{g}) + D_{KL}[\pi_\theta(a; \tilde{o}, \tilde{g}) || \pi_{ref}(a; \tilde{o}, \tilde{g})] \right] \quad (6)$$

where the reward is estimated via the binary preference classification under the Bradley-Terry preference model (Bradley & Terry, 1952):

$$\mathcal{L}(r) = -\mathbb{E}_{(\tilde{o}, \tilde{g}, a_w, a_l) \sim \tilde{\mathcal{D}}} \left[\log \sigma(r(a_w, \tilde{o}, \tilde{g}) - r(a_l, \tilde{o}, \tilde{g})) \right] \quad (7)$$

Because preference pairs (a_w, a_l) are constructed from action chunks that are aligned or misaligned with \tilde{o} , which encodes both the current visual state and future evolution through visual tracks, the learned reward function evaluates how consistent an action chunk is with the observed visual motion. Consequently, maximizing the reward, maximizing the reward encourages the policy to infer the action configurations encoded by visual tracks, thereby inducing inverse dynamics understanding within the policy model.

4.2. Instruction-Following SFT with Latent Distillation

While the track-following DPO stage strengthens visual conditioning, the target instruction-following task does not provide visual track guidance at inference. To transfer the improved vision-action alignment to instruction-following policies, we introduce a final training stage of SFT with latent-space distillation.

Specifically, given the aligned autoregressive VLA π_{align} , we freeze it as a teacher model and initialize a trainable student π_θ from its weights. We then optimize π_θ using the paired instruction and track-following \mathcal{D} and $\tilde{\mathcal{D}}$, where each track-following sample is a track-annotated counterpart of an instruction-following sample. The training objective:

$$\begin{aligned}\mathcal{L}_{\text{SFT}} &= \mathbb{E}_{(o_t, g, a_{t:t+H}) \sim \mathcal{D}} \ell_{\text{SFT}}(a_{t:t+H}, \pi_\theta(o_t, g)) \\ \mathcal{L}_{\text{Distill}} &= \mathbb{E}_{(o_t, \tilde{o}_t, g, \tilde{g}, a_{t:t+H}) \sim (\mathcal{D}, \tilde{\mathcal{D}})} \ell_{\text{sim}}(f_\theta(o_t, g), f_{\text{align}}(\tilde{o}_t, \tilde{g})) \\ \mathcal{L}_{\text{total}} &= \mathcal{L}_{\text{SFT}} + \gamma \mathcal{L}_{\text{Distill}}\end{aligned}\quad (8)$$

where ℓ_{SFT} is standard SFT loss, and ℓ_{sim} encourages the student to match the latent produced by the aligned teacher, thereby preserving the strengthened visual grounding.

Importantly, this distillation-based SFT framework allows the student π_θ to differ from π_{align} in architecture. In our experiments, π_{align} is consistently instantiated as a discrete autoregressive OpenVLA model from prior stages, while π_θ is either kept as the same or updated into a continuous parallel-decoding OpenVLA-OFT. Accordingly, ℓ_{SFT} corresponds to the discrete next-token prediction loss or the continuous $L1$ regression loss. We empirically show that this procedure consistently improves performance in both settings, which indicates that the learned vision–action alignment transfers effectively across architectures.

4.3. Implementation Details

In this work, we use off-the-shelf BootsTAPNext (Zholus et al., 2025) as the tracker. We track $N = 900$ points on an uniform grid on the image and randomly sample $n = 16$ active tracks for annotation. The DPO parameter is fixed to $\alpha = 0.1$. Unless otherwise specified, distillation loss ℓ_{sim} is set as the negative mean cosine similarity. We denote the discrete and continuous instantiation of our method as **VISTA** and **VISTA-OFT**, respectively. For VISTA, all three training stages utilize OpenVLA-7B. For VISTA-OFT, the first two stages use OpenVLA-7B, while the final stage switches to the OpenVLA-OFT-7B. We adopt LoRA (Hu et al., 2022) with rank=32 in all training.

5. Experiments

5.1. LIBERO Benchmark Evaluation

5.1.1. EXPERIMENTAL SETUPS

Evaluation Settings We first evaluate VISTA on the LIBERO manipulation benchmark (Liu et al., 2023a) to verify if our method improves visual conditioning and model performance. VISTA-OFT is excluded from this experiment and is evaluated only on the larger CALVIN benchmark (Sec. 5.2) due to its stronger expressivity. As shown in Figure 4, LIBERO consists of four suites: Spatial, Object, Goal,

and Long. Each suite contains 10 tasks, with 50 demonstrations per task for training. We preprocess the data following OpenVLA (Kim et al., 2024) to upscale the image resolution to 256×256 , exclude failure trajectories, and remove static actions. Each method is evaluated under the success rate (SR) on 500 episodes per suite (10 tasks \times 50 episodes per task). The training configuration of VISTA is detailed in Appendix A.3.

Ablation on Distillation Function We further ablate the choice of distillation loss ℓ_{sim} on LIBERO by replacing the negative cosine similarity with an L2 distance. The resulting variant is denoted as *VISTA (L2)*.

Baselines We compare against OpenVLA (Kim et al., 2024) trained with vanilla SFT under both $H = 8$ and its original $H = 1$. We additionally compare with TraceVLA (Zheng et al., 2024), which adopts the same OpenVLA architecture but augments it with historical visual trace inputs. Further state-of-the-art baselines include Diffusion Policy (Chi et al., 2023), LAPA (Ye et al., 2024), Octo (Team et al., 2024), and SpatialVLA (Qu et al., 2025). All methods are evaluated using only static third-person RGB observations.

5.1.2. EXPERIMENTAL RESULTS

For OpenVLA-8Step, VISTA, and VISTA (L2), we report the results with Receding Horizon Control (RHC), executing only the first 4 actions out of the predicted $H = 8$ before replanning. We found that RHC improves their performance in the relatively small LIBERO benchmark. Performance without RHC is reported in Appendix B.1

Overall Results. The results are summarized in Table 2. Without introducing any model architectural modifications or additional training data, VISTA consistently improves upon OpenVLA across all LIBERO suites, achieving an average SR gain of 3.1%. Coupled with the improved visual conditioning shown in Figure 2, these performance gains validate our training design and support our hypothesis that stronger visual conditioning benefits VLA performance. Moreover, VISTA surpasses other baselines including TraceVLA, justifying the performance gains from improved training recipe relative to the mere inclusion of track guidance. Overall, VISTA demonstrates competitive performance relative to all evaluated baselines.

Distillation Function Ablation Results. As shown in Table 2, VISTA (L2) variant also outperforms the baseline OpenVLA, which further demonstrate the effectiveness of our method regardless of the distillation loss instantiation. However, compared to cosine similarity, the L2 variant achieves an average SR that is 0.5% lower, with less consistent gains across task suites due to the 1.9% decrease

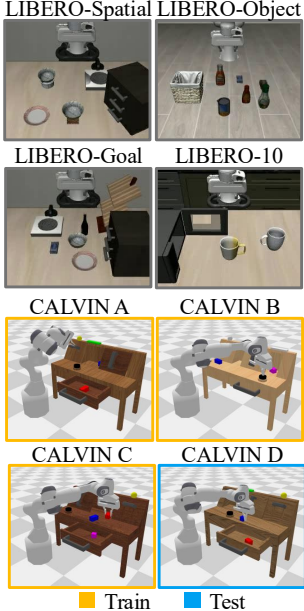


Figure 4. Illustration of benchmarks.

Table 1. CALVIN ABC→D Evaluation Results. Green (red) numbers indicate performance gains (drops) relative to the OpenVLA or OpenVLA-OFT counterpart. *Results are reproduced

Methods	Spatial	Object	Goal	Long	Mean
Diffusion Policy	78.3	92.5	68.3	50.5	72.4
Octo	78.9	85.7	84.6	51.1	75.1
LAPA	73.8	74.6	58.8	55.4	65.7
TraceVLA	84.6	85.2	75.1	54.1	74.8
SpatialVLA	88.2	89.9	78.6	55.5	78.1
OpenVLA-1Step	84.7	88.4	79.2	53.7	76.5
OpenVLA-8Step*	79.6	88.6	82.4	54.4	76.3
VISTA (L2)	87.8	89.4	80.5	58.6	<u>79.1</u>
	(+8.2)	(+0.8)	(-1.9)	(+4.9)	(+2.6)
VISTA	84.8	91.6	84.2	57.0	79.4
	(+5.2)	(+3.0)	(+1.8)	(+2.6)	(+3.1)

Table 2. LIBERO Evaluation Results. VISTA improves upon OpenVLA and outperforms a range of baseline methods. Green (red) numbers indicate performance gains (drops) relative to the OpenVLA-8Step counterpart. *Results are reproduced.

relative to OpenVLA on LIBERO-Goal. Hence, we default to the cosine similarity in remaining experiments.

5.2. Calvin Benchmark Evaluation

5.2.1. EXPERIMENTAL SETUPS

Evaluation Settings Next, we evaluate the generalization and long-horizon instruction-following capacities of VLA models on the CALVIN (Mees et al., 2022) manipulation benchmark, which comprises 4 environments (A–D) as illustrated in Figure 4. We focus on the most challenging ABC→D setting, where policies are trained on environments A–C and evaluated on D to test the generalization capacity. Our training is conducted using only the subset annotated with language instruction, which includes 17,870 episodes spanning 34 diverse tasks. Evaluation follows the

Long-Horizon Multi-Task Language Control protocol, under which the models are tested in 1000 sequences of five sequential tasks. Within each sequence, the policy must solve each new task starting from the final state of the previous, which increases difficulty due to broader state-space coverage. Performance is measured by per-task completion rate and the average task completion length. We evaluate both VISTA and VISTA-OFT, with detailed training configurations listed in Appendix. A.3.

Baselines We compare VISTA and VISTA-OFT against OpenVLA and OpenVLA-OFT to highlight the advantage of the proposed training method. We further benchmark diverse VLA designs, including RoboDual (Bu et al., 2024a), which is a cooperation system of the OpenVLA and a trained specialist, and DITA (Hou et al., 2025), which is a generalist policy based on Diffusion Transformer (DiT). Other than that, we benchmark a range of VLAs that incorporate additional action-free vision-language auxiliary tasks, including SuSIE (Black et al., 2024), CLOVER (Bu et al., 2024b), GR-1 (Wu et al., 2024), VPP (Hu et al., 2025), UniVLA (Bu et al., 2025), and ReconVLA (Song et al., 2025). Note that for RoboVLMs and VPP, we tabulate their best performance under the single static third-person view setting.

5.2.2. EXPERIMENTAL RESULTS

As shown in Table 1, our training method consistently improves both OpenVLA and OpenVLA-OFT in average length. In particular, VISTA-OFT improves the task completion rate across all tasks of OpenVLA-OFT by more than 2.3% and yields a 4% relative increase in average completion length. This suggests that our designed track-following

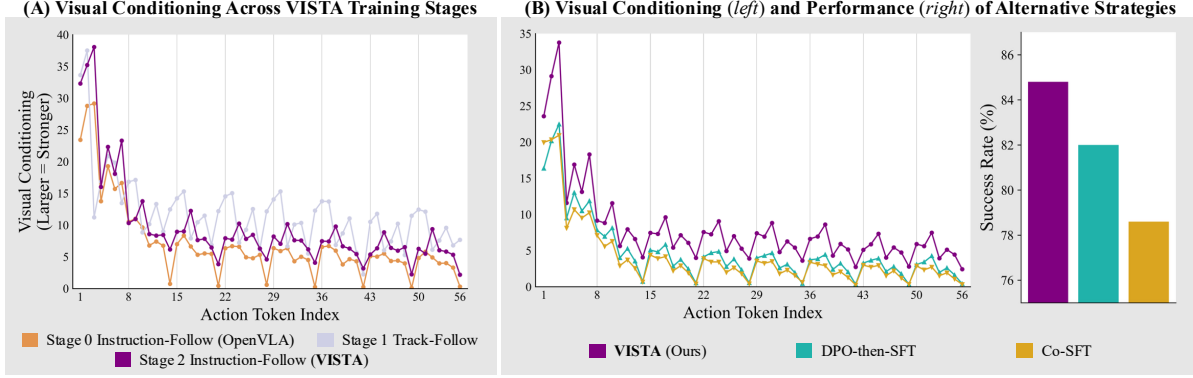


Figure 5. Analysis and Ablation on LIBERO-Spatial. (A) Change of visual conditioning during the VISTA training stages; (B) Ablation on the visual conditioning and VLA performance of alternative training strategies.

DPO extracts latents richer with vision and dynamic information, which guides better action generation. What’s more, despite relying on no external non-robotic dataset for additional pretraining or co-finetuning, VISTA-OFT surpasses a series of baselines in this category, and achieves the state-of-the-art performance in the CALVIN ABC→D benchmark. This further supports the efficacy of our training method designed to enhance visual conditioning.

5.3. Analysis and Ablation

Change of model visual conditioning during VISTA training. To examine how VISTA modulates visual conditioning in VLA models, we track its evolution across all training stages using the metric defined in Eq. 2. Specifically, we measure the visual conditioning of the discrete VISTA at each stage on a 200 randomly sampled time steps from the LIBERO-Spatial training split. Models from Stages 0 and 2 are evaluated on the instruction-following task with track-free images, while the Stage 1 model is evaluated on the track-following task with track-annotated observations.

Results are shown in Figure 5(A). The model trained solely with instruction-following SFT (Stage 0, equivalent to OpenVLA) exhibits the weakest visual conditioning, with near-zero values for some tokens, indicating complete ignorance of visual clue. Applying track-following DPO in Stage 1 substantially increases visual conditioning. Although the subsequent instruction-following training slightly reduces this effect, the final model retains markedly stronger visual conditioning than the Stage 0 baseline thanks to our distillation design. These results support our claim that VISTA improves visual grounding of the VLA model, which explains its performance gain compared to OpenVLA.

Ablation on alternative strategies. We further validate our design by comparing VISTA against two naive alternatives: (1) *DPO-then-SFT* applies track-following DPO followed by instruction-following SFT without latent dis-

tillation, analogous to a single iteration of DPO and SFT as in GRAPE (Zhang et al., 2024), and serves to validate the efficacy of adding distillation loss $\mathcal{L}_{\text{Distill}}$ as in VISTA; This baseline isolates the contribution of the distillation loss $\mathcal{L}_{\text{Distill}}$. (2) *Co-SFT*, performs a single-stage SFT on a mixture of instruction-following and track-following data, which resembles approaches that jointly train on action prediction and auxiliary world-modeling objectives.

Figure 5(B) shows visual conditioning and performance for all methods. We observe the same ordering in both metrics: VISTA achieves the highest visual conditioning and performance, followed by DPO-then-SFT, and then Co-SFT. This monotonic trend further justifies the clear correlation between visual conditioning and downstream VLA performance empirically. Co-SFT yields the weakest visual conditioning and lowest performance, indicating that naive co-training with auxiliary objectives is insufficient for improving visual grounding. While DPO-then-SFT improves upon Co-SFT, it remains inferior to VISTA, underscoring the importance of latent distillation for effectively transferring visual grounding to instruction-following policies.

6. Conclusion

Our work examines the visual conditioning in VLA, which is quantified as the impact of visual clue on the output action distribution, and show its correlation with the VLA model performance. Motivated by this finding, we further propose a VLA training recipe, named VISTA, that aligns the action prediction with the visual track guidance. Our experiments show that VISTA facilitates the visual grounding, and consistently improves the VLA performance under both the naive discrete autoregressive and the continuous parallel-decoding (i.e. OFT) configurations.

Due to compute constraints, our study focuses on the fine-tuning stage. However, we hope that this work can inspire future efforts on aligning action predictions with visual in-

puts in VLAs through extensive pretraining with mixed action-free video data, which can potentially enhance the performance and generalizability of VLA models.

Impact Statement

Our work aims to advance command-following robotic manipulation, enabling robots to physically interact with the environment in response to human instructions. Such capabilities have the potential to improve efficiency across many societal activities. By enhancing the visual dynamic understanding in a robot, our method represents a step toward more robust and reliable manipulation systems.

References

Bharadhwaj, H., Mottaghi, R., Gupta, A., and Tulsiani, S. Track2act: Predicting point tracks from internet videos enables generalizable robot manipulation. In *European Conference on Computer Vision*, pp. 306–324. Springer, 2024.

Bi, H., Tan, H., Xie, S., Wang, Z., Huang, S., Liu, H., Zhao, R., Feng, Y., Xiang, C., Rong, Y., et al. Motus: A unified latent action world model. *arXiv preprint arXiv:2512.13030*, 2025.

Black, K., Nakamoto, M., Atreya, P., Walke, H. R., Finn, C., Kumar, A., and Levine, S. Zero-shot robotic manipulation with pre-trained image-editing diffusion models. In *The Twelfth International Conference on Learning Representations*, 2024. URL <https://openreview.net/forum?id=c0chJTSbci>.

Black, K., Brown, N., Darpinian, J., Dhabalia, K., Driess, D., Esmail, A., Equi, M. R., Finn, C., Fusai, N., Gallicker, M. Y., Ghosh, D., Groom, L., Hausman, K., Ichter, B., Jakubczak, S., Jones, T., Ke, L., LeBlanc, D., Levine, S., Li-Bell, A., Mothukuri, M., Nair, S., Pertsch, K., Ren, A. Z., Shi, L. X., Smith, L., Springenberg, J. T., Stachowicz, K., Tanner, J., Vuong, Q., Walke, H., Walling, A., Wang, H., Yu, L., and Zhilinsky, U. $\pi_{0.5}$: a vision-language-action model with open-world generalization. In Lim, J., Song, S., and Park, H.-W. (eds.), *Proceedings of The 9th Conference on Robot Learning*, volume 305 of *Proceedings of Machine Learning Research*, pp. 17–40. PMLR, 27–30 Sep 2025. URL <https://proceedings.mlr.press/v305/black25a.html>.

Bradley, R. A. and Terry, M. E. Rank analysis of incomplete block designs: I. the method of paired comparisons. *Biometrika*, 39(3/4):324–345, 1952.

Brohan, A., Brown, N., Carbajal, J., Chebotar, Y., Dabis, J., Finn, C., Gopalakrishnan, K., Hausman, K., Herzog, A., Hsu, J., et al. Rt-1: Robotics transformer for real-world control at scale. *arXiv preprint arXiv:2212.06817*, 2022.

Bu, Q., Li, H., Chen, L., Cai, J., Zeng, J., Cui, H., Yao, M., and Qiao, Y. Towards synergistic, generalized, and efficient dual-system for robotic manipulation. *arXiv preprint arXiv:2410.08001*, 2024a.

Bu, Q., Zeng, J., Chen, L., Yang, Y., Zhou, G., Yan, J., Luo, P., Cui, H., Ma, Y., and Li, H. Closed-loop visuomotor control with generative expectation for robotic manipulation. *Advances in Neural Information Processing Systems*, 37:139002–139029, 2024b.

Bu, Q., Yang, Y., Cai, J., Gao, S., Ren, G., Yao, M., Luo, P., and Li, H. Univla: Learning to act anywhere with task-centric latent actions. *arXiv preprint arXiv:2505.06111*, 2025.

Chen, B., Xu, Z., Kirmani, S., Ichter, B., Sadigh, D., Guibas, L., and Xia, F. Spatialvlm: Endowing vision-language models with spatial reasoning capabilities. In *Proceedings of the IEEE/CVF Conference on Computer Vision and Pattern Recognition*, pp. 14455–14465, 2024.

Chen, Y., Xu, R., Lin, Y., and Vela, P. A. A joint network for grasp detection conditioned on natural language commands. In *International Conference on Robotics and Automation (ICRA)*, pp. 4576–4582. IEEE, 2021.

Chen, Y., Ge, Y., Tang, W., Li, Y., Ge, Y., Ding, M., Shan, Y., and Liu, X. Moto: Latent motion token as the bridging language for learning robot manipulation from videos. In *Proceedings of the IEEE/CVF International Conference on Computer Vision*, pp. 19752–19763, 2025a.

Chen, Y., Sawhney, H., Gyde, N., Jian, Y., Saunders, J., Vela, P., and Lundell, B. Schema-guided scene-graph reasoning based on multi-agent large language model system. In *The Fortieth AAAI Conference on Artificial Intelligence*, 2025b.

Chi, C., Feng, S., Du, Y., Xu, Z., Cousineau, E., Burchfiel, B., and Song, S. Diffusion policy: Visuomotor policy learning via action diffusion. In *Robotics: Science and Systems*, 2023.

Dong, S., Fu, C., Gao, H., Zhang, Y.-F., Yan, C., Wu, C., Liu, X., Shen, Y., Huo, J., Jiang, D., et al. Vita-vla: Efficiently teaching vision-language models to act via action expert distillation. *arXiv preprint arXiv:2510.09607*, 2025.

Driess, D., Springenberg, J. T., Ichter, B., Yu, L., Li-Bell, A., Pertsch, K., Ren, A. Z., Walke, H., Vuong, Q., Shi, L. X., et al. Knowledge insulating vision-language-action models: Train fast, run fast, generalize better. *arXiv preprint arXiv:2505.23705*, 2025.

Du, Y., Yang, S., Dai, B., Dai, H., Nachum, O., Tenenbaum, J., Schuurmans, D., and Abbeel, P. Learning universal policies via text-guided video generation. *Advances in neural information processing systems*, 36:9156–9172, 2023.

Geng, D., Herrmann, C., Hur, J., Cole, F., Zhang, S., Pfaff, T., Lopez-Guevara, T., Aytar, Y., Rubinstein, M., Sun, C., et al. Motion prompting: Controlling video generation with motion trajectories. In *Proceedings of the Computer Vision and Pattern Recognition Conference*, pp. 1–12, 2025.

Hancock, A. J., Wu, X., Zha, L., Russakovsky, O., and Majumdar, A. Actions as language: Fine-tuning vlms into vlas without catastrophic forgetting. *arXiv preprint arXiv:2509.22195*, 2025.

Ho, J., Jain, A., and Abbeel, P. Denoising diffusion probabilistic models. *Advances in neural information processing systems*, 33:6840–6851, 2020.

Hou, Z., Zhang, T., Xiong, Y., Duan, H., Pu, H., Tong, R., Zhao, C., Zhu, X., Qiao, Y., Dai, J., and Chen, Y. Dita: Scaling diffusion transformer for generalist vision-language-action policy. *arXiv preprint arXiv:2503.19757*, 2025.

Hu, E. J., Shen, Y., Wallis, P., Allen-Zhu, Z., Li, Y., Wang, S., Wang, L., Chen, W., et al. Lora: Low-rank adaptation of large language models. *ICLR*, 1(2):3, 2022.

Hu, Y., Guo, Y., Wang, P., Chen, X., Wang, Y.-J., Zhang, J., Sreenath, K., Lu, C., and Chen, J. Video prediction policy: A generalist robot policy with predictive visual representations. In *Forty-second International Conference on Machine Learning*, 2025. URL <https://openreview.net/forum?id=c0dhw1du33>.

Huang, W., Xia, F., Xiao, T., Chan, H., Liang, J., Florence, P., Zeng, A., Tompson, J., Mordatch, I., Chebotar, Y., et al. Inner monologue: Embodied reasoning through planning with language models. *arXiv preprint arXiv:2207.05608*, 2022.

Huang, W., Wang, C., Zhang, R., Li, Y., Wu, J., and Fei-Fei, L. Voxposer: Composable 3d value maps for robotic manipulation with language models. *arXiv preprint arXiv:2307.05973*, 2023.

Kachaev, N., Kolosov, M., Zelezetsky, D., Kovalev, A. K., and Panov, A. I. Don’t blind your vla: Aligning visual representations for ood generalization, 2025. URL <https://arxiv.org/abs/2510.25616>.

Karamcheti, S., Nair, S., Balakrishna, A., Liang, P., Kollar, T., and Sadigh, D. Prismatic vlms: Investigating the design space of visually-conditioned language models. In *Forty-first International Conference on Machine Learning*, 2024.

Kim, M. J., Pertsch, K., Karamcheti, S., Xiao, T., Balakrishna, A., Nair, S., Rafailov, R., Foster, E., Lam, G., Sanketi, P., et al. Openvla: An open-source vision-language-action model. *arXiv preprint arXiv:2406.09246*, 2024.

Kim, M. J., Finn, C., and Liang, P. Fine-tuning vision-language-action models: Optimizing speed and success. *arXiv preprint arXiv:2502.19645*, 2025.

Leng, S., Zhang, H., Chen, G., Li, X., Lu, S., Miao, C., and Bing, L. Mitigating object hallucinations in large vision-language models through visual contrastive decoding. In *Proceedings of the IEEE/CVF Conference on Computer Vision and Pattern Recognition*, pp. 13872–13882, 2024.

Li, S., Gao, Y., Sadigh, D., and Song, S. Unified video action model. *arXiv preprint arXiv:2503.00200*, 2025.

Li, X., Li, P., Liu, M., Wang, D., Liu, J., Kang, B., Ma, X., Kong, T., Zhang, H., and Liu, H. Towards generalist robot policies: What matters in building vision-language-action models. *arXiv preprint arXiv:2412.14058*, 2024.

Liu, B., Zhu, Y., Gao, C., Feng, Y., Liu, Q., Zhu, Y., and Stone, P. Libero: Benchmarking knowledge transfer for lifelong robot learning. *Advances in Neural Information Processing Systems*, 36:44776–44791, 2023a.

Liu, F., Lin, K., Li, L., Wang, J., Yacoob, Y., and Wang, L. Mitigating hallucination in large multi-modal models via robust instruction tuning. *arXiv preprint arXiv:2306.14565*, 2023b.

Mees, O., Hermann, L., Rosete-Beas, E., and Burgard, W. Calvin: A benchmark for language-conditioned policy learning for long-horizon robot manipulation tasks. *IEEE Robotics and Automation Letters*, 7(3):7327–7334, 2022.

Niu, D., Sharma, Y., Biamby, G., Quenum, J., Bai, Y., Shi, B., Darrell, T., and Herzig, R. Llarva: Vision-action instruction tuning enhances robot learning. *arXiv preprint arXiv:2406.11815*, 2024.

Ouali, Y., Bulat, A., Martinez, B., and Tzimiropoulos, G. Clip-dpo: Vision-language models as a source of preference for fixing hallucinations in lvlms. In *European Conference on Computer Vision*, pp. 395–413. Springer, 2024.

Peng, S., Yang, S., Jiang, L., and Tian, Z. Mitigating object hallucinations via sentence-level early intervention. In *Proceedings of the IEEE/CVF International Conference on Computer Vision*, pp. 635–646, 2025.

Pertsch, K., Stachowicz, K., Ichter, B., Driess, D., Nair, S., Vuong, Q., Mees, O., Finn, C., and Levine, S. Fast: Efficient action tokenization for vision-language-action models. *arXiv preprint arXiv:2501.09747*, 2025.

Qu, D., Song, H., Chen, Q., Yao, Y., Ye, X., Ding, Y., Wang, Z., Gu, J., Zhao, B., Wang, D., et al. Spatialvla: Exploring spatial representations for visual-language-action model. *arXiv preprint arXiv:2501.15830*, 2025.

Rafailov, R., Sharma, A., Mitchell, E., Manning, C. D., Ermon, S., and Finn, C. Direct preference optimization: Your language model is secretly a reward model. *Advances in neural information processing systems*, 36: 53728–53741, 2023.

Rana, K., Haviland, J., Garg, S., Abou-Chakra, J., Reid, I., and Suenderhauf, N. Sayplan: Grounding large language models using 3d scene graphs for scalable robot task planning. *arXiv preprint arXiv:2307.06135*, 2023.

Ren, J., Sundaresan, P., Sadigh, D., Choudhury, S., and Bohg, J. Motion tracks: A unified representation for human-robot transfer in few-shot imitation learning. *arXiv preprint arXiv:2501.06994*, 2025.

Shridhar, M., Manuelli, L., and Fox, D. Clipot: What and where pathways for robotic manipulation. In Faust, A., Hsu, D., and Neumann, G. (eds.), *Proceedings of the 5th Conference on Robot Learning*, volume 164 of *Proceedings of Machine Learning Research*, pp. 894–906. PMLR, 08–11 Nov 2022. URL <https://proceedings.mlr.press/v164/shridhar22a.html>.

Shridhar, M., Manuelli, L., and Fox, D. Perceiver-actor: A multi-task transformer for robotic manipulation. In *Conference on Robot Learning*, pp. 785–799. PMLR, 2023.

Shu, D., Zhao, H., Hu, J., Liu, W., Payani, A., Cheng, L., and Du, M. Large vision-language model alignment and misalignment: A survey through the lens of explainability. *arXiv preprint arXiv:2501.01346*, 2025.

Song, W., Zhou, Z., Zhao, H., Chen, J., Ding, P., Yan, H., Huang, Y., Tang, F., Wang, D., and Li, H. Reconvla: Reconstructive vision-language-action model as effective robot perceiver. *arXiv preprint arXiv:2508.10333*, 2025.

Team, O. M., Ghosh, D., Walke, H., Pertsch, K., Black, K., Mees, O., Dasari, S., Hejna, J., Kreiman, T., Xu, C., et al. Octo: An open-source generalist robot policy. *arXiv preprint arXiv:2405.12213*, 2024.

Tian, Y., Yang, S., Zeng, J., Wang, P., Lin, D., Dong, H., and Pang, J. Predictive inverse dynamics models are scalable learners for robotic manipulation. *arXiv preprint arXiv:2412.15109*, 2024.

Wang, L., Chen, X., Zhao, J., and He, K. Scaling proprioceptive-visual learning with heterogeneous pre-trained transformers. *Advances in neural information processing systems*, 37:124420–124450, 2024.

Wang, Y., Ding, P., Li, L., Cui, C., Ge, Z., Tong, X., Song, W., Zhao, H., Zhao, W., Hou, P., et al. Vla-adapter: An effective paradigm for tiny-scale vision-language-action model. *arXiv preprint arXiv:2509.09372*, 2025a.

Wang, Y., Li, X., Wang, W., Zhang, J., Li, Y., Chen, Y., Wang, X., and Zhang, Z. Unified vision-language-action model. *arXiv preprint arXiv:2506.19850*, 2025b.

Wen, C., Lin, X., So, J., Chen, K., Dou, Q., Gao, Y., and Abbeel, P. Any-point trajectory modeling for policy learning, 2023.

Wu, H., Jing, Y., Cheang, C., Chen, G., Xu, J., Li, X., Liu, M., Li, H., and Kong, T. Unleashing large-scale video generative pre-training for visual robot manipulation. In *The Twelfth International Conference on Learning Representations*, 2024. URL <https://openreview.net/forum?id=NxoFmGgWC9>.

Yang, Z., Chen, Y., Wang, J., Manivasagam, S., Ma, W.-C., Yang, A. J., and Urtasun, R. Unisim: A neural closed-loop sensor simulator. In *Proceedings of the IEEE/CVF Conference on Computer Vision and Pattern Recognition*, pp. 1389–1399, 2023.

Ye, S., Jang, J., Jeon, B., Joo, S., Yang, J., Peng, B., Mandlekar, A., Tan, R., Chao, Y.-W., Lin, B. Y., et al. Latent action pretraining from videos. *arXiv preprint arXiv:2410.11758*, 2024.

Yuan, Y., Cui, H., Huang, Y., Chen, Y., Ni, F., Dong, Z., Li, P., Zheng, Y., and Hao, J. Embodied-r1: Reinforced embodied reasoning for general robotic manipulation. *arXiv preprint arXiv:2508.13998*, 2025.

Zawalski, M., Chen, W., Pertsch, K., Mees, O., Finn, C., and Levine, S. Robotic control via embodied chain-of-thought reasoning. *arXiv preprint arXiv:2407.08693*, 2024.

Zhang, J., Guo, Y., Hu, Y., Chen, X., Zhu, X., and Chen, J. Up-vla: A unified understanding and prediction model for embodied agent. *arXiv preprint arXiv:2501.18867*, 2025.

Zhang, Z., Zheng, K., Chen, Z., Jang, J., Li, Y., Han, S., Wang, C., Ding, M., Fox, D., and Yao, H. Grape: Generalizing robot policy via preference alignment. *arXiv preprint arXiv:2411.19309*, 2024.

Zhao, Q., Lu, Y., Kim, M. J., Fu, Z., Zhang, Z., Wu, Y., Li, Z., Ma, Q., Han, S., Finn, C., et al. Cot-vla: Visual chain-of-thought reasoning for vision-language-action

models. In *Proceedings of the Computer Vision and Pattern Recognition Conference*, pp. 1702–1713, 2025.

Zhao, Z., Wang, B., Ouyang, L., Dong, X., Wang, J., and He, C. Beyond hallucinations: Enhancing lmlms through hallucination-aware direct preference optimization. *arXiv preprint arXiv:2311.16839*, 2023.

Zheng, R., Liang, Y., Huang, S., Gao, J., Daumé III, H., Kolobov, A., Huang, F., and Yang, J. Tracevla: Visual trace prompting enhances spatial-temporal awareness for generalist robotic policies. *arXiv preprint arXiv:2412.10345*, 2024.

Zholus, A., Doersch, C., Yang, Y., Koppula, S., Patraucean, V., He, X. O., Rocco, I., Sajjadi, M. S., Chandar, S., and Goroshin, R. Tapnext: Tracking any point (tap) as next token prediction. *arXiv preprint arXiv:2504.05579*, 2025.

Zhou, Y., Cui, C., Rafailov, R., Finn, C., and Yao, H. Aligning modalities in vision large language models via preference fine-tuning. *arXiv preprint arXiv:2402.11411*, 2024a.

Zhou, Y., Fan, Z., Cheng, D., Yang, S., Chen, Z., Cui, C., Wang, X., Li, Y., Zhang, L., and Yao, H. Calibrated self-rewarding vision language models. *Advances in Neural Information Processing Systems*, 37:51503–51531, 2024b.

Zhou, Z., Zhu, Y., Zhu, M., Wen, J., Liu, N., Xu, Z., Meng, W., Peng, Y., Shen, C., Feng, F., et al. Chatvla: Unified multimodal understanding and robot control with vision-language-action model. In *Proceedings of the 2025 Conference on Empirical Methods in Natural Language Processing*, pp. 5377–5395, 2025.

A. Additional Implementation Details

A.1. Visual Track Generation Details

This section provides additional details on visual track generation. We adopt different strategies for LIBERO and CALVIN benchmarks. For LIBERO, we follow the protocol in TraceVLA (Zheng et al., 2024) to track over overlapping video segments. Specifically, each demonstration is divided into overlapping segments of 32 size (e.g. [1, 32], [17, 48], etc). For each segment, we initialize $N = 900$ tracking points in the first frame of the segment and track their coordinates throughout the entire 32-frame window. With this design, any track whose starting frame falls within the first 16 frames of a segment is guaranteed to have a future trajectory of at least 16 frames. This design also enables the inclusion of newly visible regions and increases diversity of visual tracks across segments. For Calvin, since each language-annotated demonstration has a maximum length of 64 frames, we directly track the initialized points over the entire trajectory without further segmentation.

To obtain valid and active visual tracks, we apply several filtering criteria. First, we remove static points by calculating frame-to-frame pixel displacement over the tracking interval (32 frames for LIBERO and up to 64 frames for CALVIN). Points with an average displacement below 2 pixels are discarded. Next, we remove points that exhibit insufficient temporal motion consistency, defined as having displacements greater than 2 pixels in fewer than one quarter of the tracked frames. Finally, we discard points that exhibit abrupt motion, specifically those with a displacement exceeding 10 pixels between any pair of consecutive frames. This filtering strategy effectively removes false-positive tracks, particularly those with spurious jumps.

We provide qualitative demonstrations of the annotated visual tracks in Figure 6 (LIBERO) and Figure 7 (CALVIN).

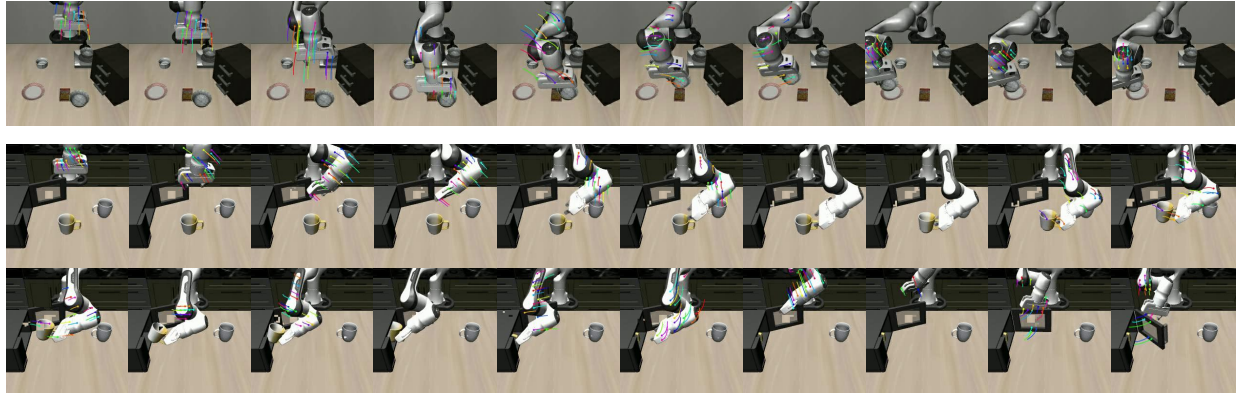


Figure 6. Track annotation results on LIBERO dataset. Top: LIBERO-Spatial; Bottom: LIBERO-Long. Best viewed when zoomed in!

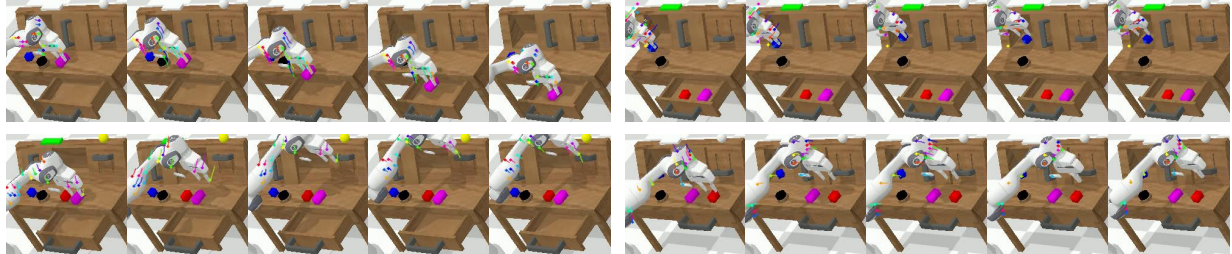


Figure 7. Track annotation results on CALVIN dataset. We select 4 sequences for visualization. Best viewed when zoomed in!

A.2. VLA Prompt

Given a task such as:

[TASK] pick up the black bowl between the plate and the ramekin and place it on the plate

The instruction-following prompt g and track-following prompt \tilde{g} are:

[Instruction-following Prompt] What 8 step actions should the robot take to [TASK] **[Track-following Prompt]** The visual trajectory depicts a way to [TASK]. What 8 step actions should the robot take to follow it?

A.3. Training Configuration Details

VISTA training configurations We show VISTA training configurations for all experiments in Table 3.

Experiment	Optimizer	Scheduler	LoRA Rank	Global Batch Size	GPU [†] Count	Learning Rate	Total Steps/Epochs
LIBERO	Stage 0	Adam	Constant	32	128	8	60K Steps (others) 80K Steps (Long)
	Stage 1	Adam	Constant	32	16	4	60K Steps
	Stage 2	Adam	Constant	32	96	8	20K Steps (Spatial, Goal) 30K Steps (Object, Long)
CALVIN	Stage 0	Adam	Constant	32	128	8	200K Steps
	Stage 1	Adam	Constant	32	48	8	5 Epochs
	Stage 2	Adam	Constant	32	96 (VISTA) 64 (VISTA-OFT)	8	12 Epochs (VISTA) 6 Epochs (VISTA-OFT)

Table 3. VISTA Training Configurations. [†] We use NVIDIA A100 for all of our training experiments.

Baseline OpenVLA/OpenVLA-OFT reproduction details For 8-Step OpenVLA (Kim et al., 2024), we use the VISTA Stage 1 model in all experiments since they are equivalent. For OpenVLA-OFT (Kim et al., 2025), which is also 8-step, we tabulate the LIBERO results directly from the original paper. For CALVIN, we train OpenVLA-OFT for 6 epochs with global batch size of 64. We observe that *OpenVLA-OFT does not benefit from longer training*. When increasing the training epochs from 6 to 12, OpenVLA-OFT performance in CALVIN ABC→D drops from 3.868 to 3.861.

Alternative training strategies details. Here we summarize the training details of the alternative approaches shown in Figure 5 (B). For DPO-then-SFT, we follow the same configuration as VISTA in LIBERO-Spatial. For Co-SFT, we train the model for 100K steps, which is 40K steps more than the OpenVLA to accommodate the auxiliary task and additional training data.

B. Additional Results

B.1. LIBERO Results without Receding Horizon Control

Methods	Plan-Execute Horizon	Spatial	Object	Goal	Long	Mean
OpenVLA	8-8	73	84.2	72	52.8	70.5
	8-4	79.6	88.6	82.4	54.4	76.3
VISTA	8-8	75.8	87.6	81.4	49.4	73.5
	8-4	(+2.8)	(+3.4)	(+9.4)	(-3.4)	(+3)
	8-8	84.8	91.6	84.2	57.0	79.4
	8-4	(+5.2)	(+3.0)	(+1.8)	(+2.6)	(+3.1)

Table 4. LIBERO Results without Receding Horizon Control. Green (red) numbers indicate performance gains (drops) relative to the OpenVLA counterpart.

We show the performance of OpenVLA and VISTA with and without the Receding Horizon Control (RHC) in Table 4. In both settings, VISTA improves OpenVLA by at least 3% in success rate, which further proves the effectiveness of our approach. In addition, removing RHC leads to a performance drop for both VISTA and OpenVLA in LIBERO. This degradation is potentially due to the declining visual conditioning when predicting later action tokens as illustrated in Figure 2, which suggests that the later tokens are less reliable. In that regime, action prediction becomes more dominated by the

action distribution prior learnt from the dataset, which makes them less grounded on the world observations. However, we do not observe performance gain by adding RHC in CALVIN. A plausible explanation is that the CALVIN training dataset is substantially larger than LIBERO, which may mitigate overfitting to action priors and support more stable long-horizon action prediction.

B.2. Visual conditioning in other LIBERO suites

In addition to Figure 2, we illustrate our quantified visual conditioning of OpenVLA and VISTA model in the remaining LIBERO suites in Figure 8 following the protocol in Sec. 3.2. We make two observations from the plots. First, the successful trials of OpenVLA constantly feature stronger visual grounding compared to failure ones across all suites, which further support our claim on the importance of visual clue utilization to the performance of VLA. Second, VISTA improves the visual conditioning of all action tokens in LIBERO-Goal as in LIBERO-Spatial. As for LIBERO-Object and LIBERO-Long, although the visual conditioning is not improved in the prediction of later tokens, it is enhanced to the level of the average successful OpenVLA rollouts at the early stage of the prediction as highlighted by the goal bounding box. Coupled with Receding Horizon Control (RHC), the performance is improved as presented in Table 2. However, the inability to raise visual conditioning at the later stage might explain the degraded performance of VISTA without RHC in Table 4, which is left for future work.

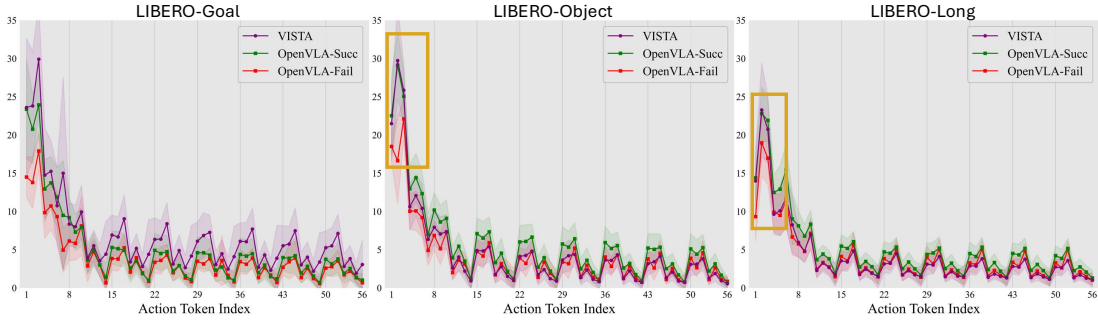


Figure 8. Visual Conditioning of VISTA and OpenVLA in more LIBERO Suites. Left: LIBERO-Goal; Middle: LIBERO-Object; Right: LIBERO-Long.

B.3. Ablation on the Distillation Loss Weight

We ablate on the distillation loss weight γ on LIBERO-Spatial. We experiment on $\gamma \in [0.01, 0.1, 1]$ in VISTA Stage 3 training, where all training configurations are the same as the ones tabulated in Table 3, except that we reduce the global batch size from 96 to 48 to reduce the required GPU from 8 to 4 to save compute. We also evaluate on 200 trials instead of 500 as in the main paper. As shown in Table 5, although VISTA with all γ outperforms OpenVLA (presented in Table 4), $\gamma = 0.1$ achieves the best result. Hence we fix $\gamma = 0.1$ in all main experiments.

Plan-Execute Horizon	γ		
	0.01	0.1	1
8-8	72	76	73
8-4	81.5	86	85

Table 5. LIBERO-Spatial Success Rate (%) under Different Distillation Loss Weight γ .